Observation of d(t,n) Neutrons Following d(d,p)t Reactions in a Deuterium Gas Cell: An Attempt to Repeat Ruhlig's 1938 Observation of Secondary Reactions

Lestone, John Paul
Tornow, Werner
Chadwick, Mark Benjamin
Wilhelmy, Jerry B.
Finch, S.
Friesen, F.
Mancil, E.

To be published in: Fusion Science and Technology

DOI to publisher's version: 10.1080/15361055.2024.2342484

Fusion Science and Technology

ISSN: (Print) (Online) Journal homepage: www.tandfonline.com/journals/ufst20

Observation of d(t,n)α Neutrons Following d(d,p)t Reactions in a Deuterium Gas Cell: An Attempt to Repeat Ruhlig's 1938 Observation of Secondary Reactions

J. P. Lestone, S. Finch, F. Friesen, E. Mancil, W. Tornow, J. B. Wilhelmy & M. B. Chadwick

To cite this article: J. P. Lestone, S. Finch, F. Friesen, E. Mancil, W. Tornow, J. B. Wilhelmy & M. B. Chadwick (11 Jun 2024): Observation of d(t,n)α Neutrons Following d(d,p)t Reactions in a Deuterium Gas Cell: An Attempt to Repeat Ruhlig's 1938 Observation of Secondary Reactions, Fusion Science and Technology, DOI: 10.1080/15361055.2024.2342484

To link to this article: https://doi.org/10.1080/15361055.2024.2342484

Published online: 11 Jun 2024.

FUSION SCIENCE AND TECHNOLOGY

DOI: https://doi.org/10.1080/15361055.2024.2342484

Observation of d(t,n)α Neutrons Following d(d,p)t Reactions in a Deuterium Gas Cell: An Attempt to Repeat Ruhlig's 1938 Observation of Secondary Reactions

J. P. Lestone,[a]* S. Finch,[b] F. Friesen,[b] E. Mancil,[b] W. Tornow,[b] J. B. Wilhelmy,[a] and M. B. Chadwick[a]

[a]*Los Alamos National Laboratory, Los Alamos, New Mexico 87545*
[b]*Duke University and Triangle Universities Nuclear Laboratory, Durham, North Carolina 27708*

Received January 24, 2024
Accepted for Publication April 6, 2024

Abstract — *In order to benchmark methods used to calculate reaction-in-flight fusion reactions in inertial confinement fusion and address issues related to the first claimed observation of d(t,n)α reactions in 1938, secondary d(t,n)α reactions have been observed following d(d,p)t reactions in deuterium gas. A pulsed 200-nA, 2.2-MeV deuterium beam from the Triangle Universities Nuclear Laboratory FN tandem accelerator was injected into a cylindrical multiatmosphere deuterium gas target. The incident beam traversed along the target cylinder's 3-cm symmetry axis after its passage through a Havar entrance foil. Two different Havar foil thicknesses were used to obtain 1.5- and 0.6-MeV deuteron beams entering the deuterium cell. The cylinder's radius was 2 cm to allow for d(d,p)t tritons emitted perpendicular to the beam to range out in the deuterium gas. The neutron emission from the cell was observed via its time of flight to a liquid scintillator placed at various angles to the beam direction, at a distance of 243 cm. Pulse-shape-discrimination techniques were used to separate neutron and gamma-ray signals seen in the liquid scintillator. The observed probability of ~2 × 10^{-4} for inducing secondary d(t,n)α fusion in the gas cell per d(d,p)t reaction is consistent with theoretical expectations.*

Keywords — *Deuterium gas cell, d(t, n)α neutrons, d(d, p)t reactions, Ruhlig's 1938 experiment.*

Note — *Some figures may be in color only in the electronic version.*

I. INTRODUCTION

Reaction-in-flight (RIF) fusion is the process by which fast-moving (nonthermal) fusible ions undergo fusion while slowing down inside a medium containing fusible nuclei. Nonthermal fusible ions can be generated by several mechanisms including the scattering of fusion neutrons by fusible ions and the charged particle products of fusion reactions. For example, in inertial confinement fusion (ICF), 14-MeV fusion neutrons can elastically scatter from deuterium or tritium ions to generate several mega-electron-volt ions that can induce additional fusions in the surrounding material. This process can generate deuteron plus triton (dt)–fusion neutrons that have energies far from the nominal 14-MeV value in the laboratory frame. Observations of these RIF neutrons have been used to test ion stopping powers in plasmas.[1] When a fast charged particle from an initial fusion reaction initiates an additional fusion reaction before the slowing of the charged particle to thermal energies, the additional fusion events are labeled "secondary reactions." Except for a short 1938 paper by Ruhlig[2]—though such reactions have been studied in ICF experiments[3]—we are unaware of any observations of secondary fusion

*E-mail: lestone@lanl.gov

reactions following initial d(d,p)t reactions in a well-defined room temperature environment.

While looking for low-lying excited states in ^{3}He nuclei in 1938, Ruhlig inferred the presence of dt-fusion neutrons following the fusion of 0.5-MeV deuterons incident on deuterated phosphoric acid (D_3PO_4). Ruhlig correctly concluded that high-energy neutrons can be generated by secondary d(t,n)α reactions following d(d,p)t reactions in a deuterated target. In Ruhlig's experiment, he monitored the rate of secondary d(t,n)α reactions via the presence of high-energy protons (>15 MeV) generated by the scattering of neutrons from a cellophane foil and the rate of the initiating d(d,p)t reactions via the rate of the sister reaction d(d,n)^{3}He. The d(d,n) rate was monitored by the scattering of low-energy protons (<4 MeV) out of the same cellophane foil mentioned above. Ruhlig reported about 1 high-energy proton per 1000 low-energy protons and then correctly concluded that the d(t,n)α reaction must be "an exceedingly probable one." However, a recent analysis of Ruhlig's experiment concluded that Ruhlig's 1:1000 ratio was optimistically high or perhaps caused by secondary d(^{3}He,p)α reactions.[4] In order to test the methods used to calculate secondary reaction probabilities to the 10% to 20% level, we decided to make a modern measurement of secondary dt-fusion probabilities following deuteron-deuteron (dd) fusion in a well-defined geometry. A more accurate test is likely hindered by uncertainties in stopping powers at low energies.

At first, we hoped to perform a measurement very similar to that of Ruhlig's 1938 experiment, with a 0.5-MeV deuteron beam incident on a D_3PO_4 target. However, several experimental difficulties, including that the 0.5-MeV d+D_3PO_4 secondary dt-fusion probability does appear to be $<10^{-4}$ as implied by recent calculations,[4] resulted in the failure of our originally planned experiments, owing to low statistics relative to the background rates. So, instead, we conducted easier experiments with 1.5-MeV deuterons incident on a deuterium gas cell. Without the phosphorus and oxygen contained in the D_3PO_4 target, the dt-fusion probability (in deuterium gas) is calculated to increase by a factor of about 5 (relative to the D_3PO_4 case), and the higher dd-fusion rate (with 1.5-MeV deuterons instead of 0.5-MeV deuterons) increases the experimental reaction rate by a further factor of about 10. This increase in the absolute secondary dt-fusion rate enabled several difficulties to be overcome in a timely manner.

With these issues resolved, we then embarked on the longer measurements needed to observe the secondary dt fusions following 0.6-MeV deuterons incident into our deuterium gas cell. Since our successful measurements with a deuterium gas cell, measurements with solid deuterated polyethylene (CD_2), liquid heavy water (D_2O), and liquid deuterated phosphoric acid targets were completed as this paper was being finalized. These results will be reported at a later date.[5]

Here, we used pulsed 2.22-MeV deuterons from the Triangle Universities Nuclear Laboratory (TUNL) FN tandem accelerator[6] to induce dd-fusion reactions in a 4-atm deuterium gas cell with the aim of observing secondary dt-fusion reactions. Approximately one-half of the internal dd fusions generate fast-moving tritons that are capable of inducing dt fusion in the deuterium gas cell. In this relatively simple experiment, the probability that an initial d(d,p)t reaction is followed by a secondary d(t,n)α reaction is governed by a combination of the experimental setup, the relevant fusion cross sections, and the stopping powers of tritons in the deuterium gas cell. Given that fusion cross sections are very well known, our experiment could be viewed as a test of low-energy stopping powers of tritons in a deuterium gas. The theory of the energy loss of charged particles transiting atomic matter traces its origin to theoretical studies first performed by Bethe.[7]

II. EXPERIMENTAL SETUP

The experimental setup used here is depicted by a combination of Figs. 1 and 2. The 4.05-atm deuterium gas cell (see Fig. 1) was a cylindrical tantalum can with an inner gas length of 3 cm and a diameter of 4 cm. The symmetry axis of the cylinder was aligned with the beam axis. Our 200-nA beam of pulsed 2.22-MeV deuterons first passed through a Havar entrance window that separated the gas cell from the vacuum of the accelerator beamline. The TUNL lithium carbide neutron time-of-flight (TOF) spectrometer shield[8] (see Fig. 2) was needed to reduce the neutron and gamma-ray room return reaching the 3.5 × 2-in. NE218 liquid scintillator[9] coupled to a Phillips 58DVP photomultiplier tube. At first, we used a Havar foil thickness of ¼ mil to degrade the deuteron beam to a kinetic of 1.5 MeV on exiting the foil and incident into the gas cell.

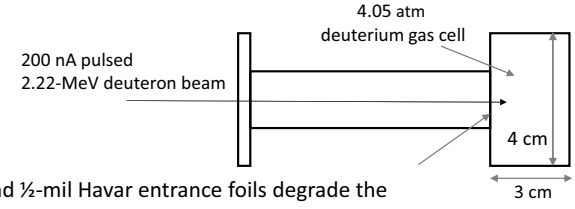

Fig. 1. A depiction of the 3-cm-length × 4-cm-diameter cylindrical gas cell that can be bolted to the end of a beamline at the TUNL FN tandem accelerator.[6]

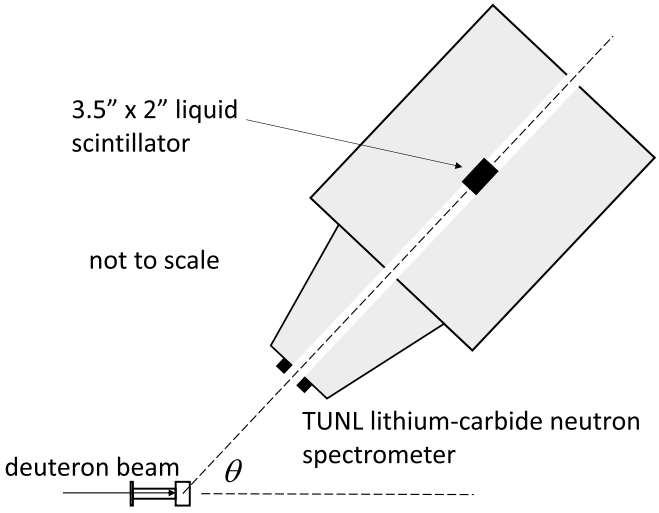

Fig. 2. The gas cell from Fig. 1 is shown in the bottom-left part of this figure. The TUNL lithium carbide neutron spectrometer[8] is depicted at an angle θ to the beam direction. The center of the 3.5 × 2-in. liquid scintillator was 243 cm from the center of the gas cell.

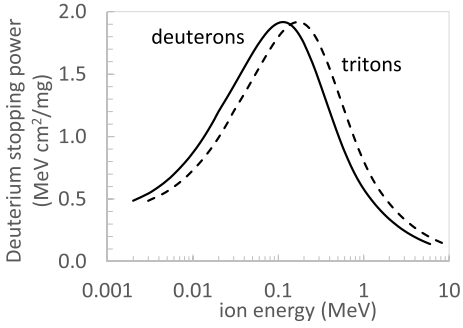

Fig. 3. The stopping power for deuterons (solid curve) and tritons (dashed curve) in deuterium, obtained by modifying the proton on hydrogen gas stopping powers from PSTAR[10] as discussed in the text.

Of particular importance to the present study is the stopping powers of deuterons and tritons passing through deuterium. These are displayed in Fig. 3 and obtained via the National Institute of Standards and Technology (NIST).[10] Our deuteron tables (for protons slowing in deuterium) are obtained by dividing the NIST hydrogen stopping powers by 2. This is because the deuterium gas has the same electronic (stopping) configuration but with twice the nuclear mass of hydrogen gas. The corresponding stopping powers for deuterons and tritons are obtained via the proton values but at the same ion velocities by multiplying the proton energies by the mass ratio to the ion of interest.

After the refinement of our experimental methods, we then switched to a thicker ½-mil Havar foil, with a corresponding deuteron energy of 0.6 MeV incident on the gas. The average energy of the incident deuterons is

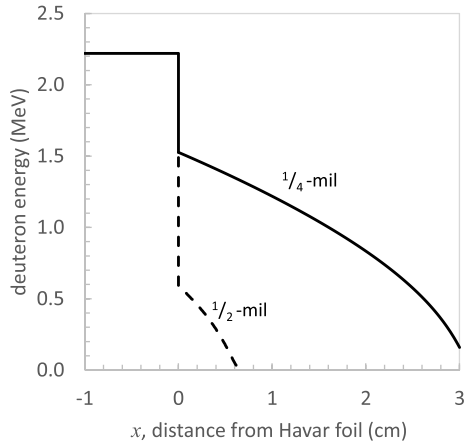

Fig. 4. The passage of a 2.22-MeV deuteron beam through ¼-mil (solid curve) and ½-mil (dashed curve) Havar foils (at $x = 0$) and then into the 4.05-atm deuterium gas cell ($x > 0$).

displayed in Fig. 4 as a function of their location in the deuterium gas cell, for both the ¼- and ½-mil Havar foil cases. For the ¼-mil case, the beam is almost brought to rest inside the deuterium gas and impinges on the tantalum end of the gas cell with an energy of ~0.2 MeV. For the thicker (½-mil) Havar foil, the beam is brought to rest ~0.7 cm inside the gas cell.

Given the slowing deuteron beam properties presented in Fig. 4, the only additional information required to calculate the probability of inducing a dd-fusion reaction is the energy dependence of the corresponding cross sections displayed in Fig. 5. For convenience, we here

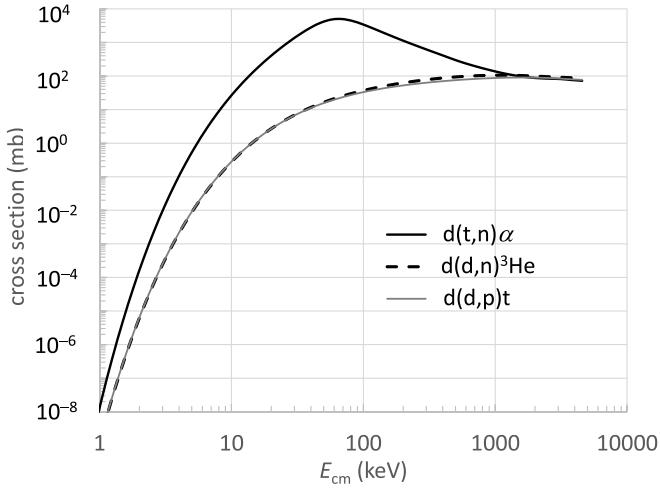

Fig. 5. The modern fusion cross sections used here as a function of the kinetic energy in the center-of-mass frame, obtained using the formulas given by Bosch.[11] The d(d,n) and d(d,p) fusion cross sections are similar in magnitude while the d(t,n) cross sections (used later in this paper) have a large resonant enhancement (5 b at ~65 keV).

use the fusion cross-section formulas of Bosch.[11] These are known to be near to the corresponding ENDF/B-VIII evaluations.[12] To calculate dd-fusion probabilities, we divide the deuteron's range (in areal density) into about 100 uniform steps of *dx* and estimate the probability for d(d,p)t and d(d,n)^{3}He fusion reactions across each step using

$$dP = dx \cdot \frac{N_A \sigma(E_d)}{A_d}, \quad (1)$$

where A_d = 2.014 g/mole = atomic mass of deuterons; N_A = Avogadro's number; $\sigma(E_d)$ = average cross section across the areal density step in question. For the ¼-mil Havar foil case, integrating across the areal densities along the path of an incident deuteron gives d(d,p)t and d(d,n)^{3}He probabilities of 4.38 × 10^{-5} and 5.40 × 10^{-5} per incident deuteron, respectively. The corresponding probabilities for the ½-mil foil case are 5.56 × 10^{-6} and 6.59 × 10^{-6}, respectively. The corresponding average laboratory energies of the fusion-inducing deuterons are ~1.04 MeV (¼ mil) and ~0.3 MeV (½ mil), with these reactions occurring about 1.5 and 0.4 cm inside the gas cell. However, in relation to the present experiment, in regard to the d(d,n)^{3}He neutron emission, it is more useful to consider the location where one-half of the fusions occurs on either side. For the ¼-mil case, this is at a depth of ~1.3 cm inside the gas cell where the incident deuterons have slowed to 1.14 MeV. The neutrons from the d(d,n)^{3}He reactions occurring at this location with angles to the beam direction (in the laboratory frame) of 0, 45, 90, and 120 deg are 4.3, 3.8, 2.7, and 2.2 MeV, respectively.

III. EXPERIMENTAL RESULTS

The observed TOF spectra of d(d,n) neutrons at angles of θ deg = 0, 45, 90, and 120 deg, with the ¼-mil Havar foil are displayed in Fig. 6. The 2-h runs at each neutron angle were with a 2-ns-wide pulsed deuteron beam every 400 ns, with a typical time-averaged current on target of ~200 nA. If the TOF resolution was infinitely small and the beam pulse infinitely narrow, then the TOF spectrum (for each angle) would peak sharply on the left-hand side of the TOF peak, corresponding to the shortest TOFs associated with the d(d,n) reactions just beyond the Havar foil where the incident deuteron ions are at their highest energy in the gas. The shapes of the left-hand side of the TOF peaks (in Fig. 6) give a total system one-sigma timing resolution of 2.5 ns. To the right

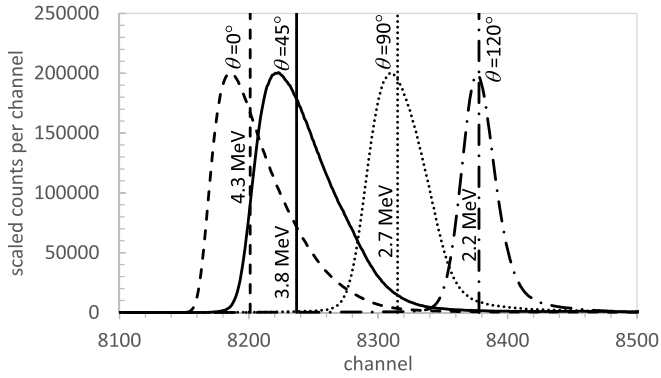

Fig. 6. The TOF spectra of d(d,n) neutrons with the ¼-mil Havar foil, at θ = 0 deg (dashed), 45 deg (solid), 90 deg (dotted), and 120 deg (dash-dotted). The vertical line shows the locations that divide the spectra into two equal-intensity regions. The corresponding calculated neutron energies are indicated. The non-0-deg spectra are here scaled to match the maximum intensity of the 0-deg data.

of these peaks, the TOF spectra fall monotonically, governed by a combination of the degrading energy of the incident deuteron ions and the decreasing d(d,n) cross section with decreasing deuteron energy. At forward angles (see θ = 0 deg and 45 deg in Fig. 6), the finite TOF resolution and finite pulse width smear out the peak, but it remains on the left-hand side of the TOF peak with a noticeable skewness to the right. At larger angles (see θ = 90 deg and 120 deg in Fig. 6), the neutron laboratory energies are not boosted to higher values (in the transformation from the center-of-mass to laboratory frames), and thus, the spread in the TOF values due to the different d(d,n) locations (and thus different deuteron speeds along the symmetry axis of the gas cell) is smaller than that for the forward angle neutrons. With the smaller spread in mid-angle neutron TOFs, the finite resolution of the TOF system gives a more symmetric peak. This makes the quantitative use of the location of the maximum in the TOF peak complex, and we instead use the TOF locations displayed by the vertical lines in Fig. 6, which denote the positions with one-half of the observed events on either side, to denote an effective neutron energy for each of the angles. These neutron-TOF channel locations are indicated by the vertical lines in Fig. 6 and are plotted versus the TOF of these neutrons in Fig. 7. The calculated d(d,n) TOFs in Fig. 7 are obtained using the effective energies discussed above and the distance from the center of the gas to the center of the liquid scintillator.

A TOF calibration was obtained using neutrons of known energies from d(t,n) reactions on a thin tritiated target at two different angles: the location of a TOF

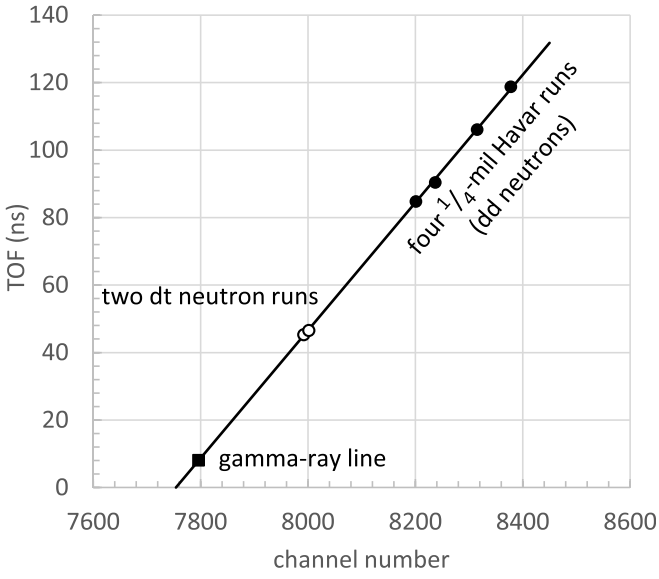

Fig. 7. The TOF calibration using two d(t,n) neutron energies obtained using our deuteron beam on a thin tritium target (open circles) and a gamma-ray TOF peak induced by the interaction of the beam with the Havar entrance window (square). The black line shows the extrapolation of the TOF calibration to the slower d(d,n) neutrons. The solid circles display the effective locations of the d(d,n) neutrons (see text) with the ¼-mil Havar foil observations of $\theta = 0$, 45, 90, and 120 deg (see Fig. 6).

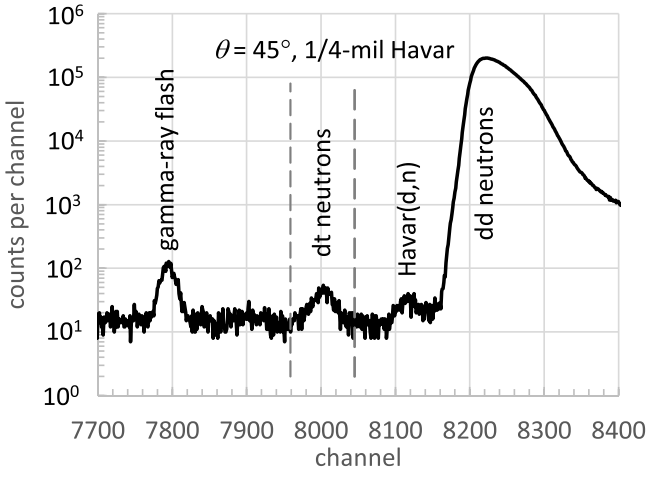

Fig. 8. The TOF spectrum at $\theta = 45$ deg with the ¼-mil Havar foil.

gamma-ray peak induced by the deuteron beam passing through the Havar entrance foil (see Fig. 8) and the known calibration of 5.284 TOF channels per nanosecond. The extrapolation of this calibration (see the line in Fig. 7) is consistent with the d(d,n) data displayed is Fig. 6 (solid circles). This adds confidence to the validity of our TOF calculation.

The TOF spectrum of $\theta = 45$ deg with the ¼-mil Havar foil is shown in Fig. 8, which corresponds to the 45-deg data set displayed in Fig. 6, but now unscaled and with the vertical axis displayed logarithmically so that the faster rarer particles can be seen in the same figure. There are three features associated with faster particles. The fastest peak near channel 7800 is due to gamma rays induced by the deuteron beam transiting the Havar foil. The displayed TOF spectrum is nominally due to neutrons obtained by setting a pulse-shape-discrimination (PSD) region dominated by neutrons incident on the liquid scintillator. However, the gamma-ray flash is intense, and a small fraction of these events bleeds through into the neutron PSD region. The peak about channel 8000 is due to the secondary dt-fusion neutrons of interest to the present study. This peak is significantly broader than those seen with our deuteron beam incident on the thin tritiated target used to calibrate the TOF system. This widening of the secondary dt-fusion neutron TOF peaks is due to the broad range of triton directions and energies involved in the secondary dt-fusion reactions. The peak/shoulder near 8100 is due to high-energy neutrons (~10 MeV) generated by (d,n) reactions with some of the isotopes in the Havar foil. A run with the deuterium gas replaced with helium confirmed these hypotheses, with the gamma-ray flash and Havar (d,n) features remaining while the peaks associated with dd-fusion and dt-fusion neutrons disappeared.

To obtain the observed number of dt-fusion neutrons, the background under and about the dt-fusion peak was assumed to vary linearly with time. Background regions about ten channels wide on either side of the dt-fusion peak were set by eye. Readers might be interested to know that in an earlier experiment (not reported here), we attempted to observe the secondary dt-fusion neutrons with a ¼-mil Havar foil but without the large lithium carbide TOF spectrometer depicted in Fig. 2. In this case, the room return was such that the background about the dt-fusion neutron peaks was 10^3 lower than the height of the dd-fusion neutron peaks instead of the ratio of 10^4 obtained in the present experiment (see Fig. 8). In the experiment without the large TOF lithium carbide spectrometer, the secondary dt-fusion neutrons could be seen, but only with a significant reduction in the background obtained by placing a high pulse-height threshold of the neutron detector. This led to a reduction in the number of observable dt-fusion neutrons and additional uncertainties associated with the threshold dependence of the neutron detector efficiency as a function of pulse-height threshold. This poorer experiment gave a secondary dt-fusion probability in agreement with the present study but with an uncertainty of 40%. The desire

to reduce the experimental uncertainty to the 10% to 20% level led to the experiment described here.

To obtain values proportional to the dd-fusion and dt-fusion neutrons generated, the number of observed neutrons was divided by the beam current integrator (BCI) for each run and the known efficiency of the liquid scintillator[9] for the corresponding effective neutron energy of the observed TOF peak. A ^{137}Cs source was used to set the detector threshold to 0.37 times the corresponding Compton edge. Efficiency curves with thresholds from 0.5 to 7.0 times the Cs edge were extrapolated to our value of 0.37 (see Fig. 9). The efficiency curves of Ref. [9] were obtained by a combination of modeling and experiment, with these being consistent at the level of a few percent.

The corresponding experimental results at the four observed angles for both Havar foil thicknesses are displayed in Fig. 10. The d(d,n) reactions have a noticeable angular distribution as expected.[13] The d(t,n) angular distributions are relatively flat in the center-of-mass frame.[12] Averaging these angular distributions over the wide range of triton directions leads to an even flatter secondary dt-fusion neutron angular distribution relative to the direction of the incident deuteron beam, as observed (see Fig. 10). When integrating the observed d(t,n) angular distribution to estimate the total intensity of the secondary d(t,n) neutrons, we here assume that the secondary dt-fusion neutron angular distribution is isotropic in the laboratory frame.

Integrating the d(d,n) and d(t,n) angular distributions displayed by the curves in Fig. 10 leads to d(t,n) to d(d,n) ratios of $(1.4 \pm 0.2) \times 10^{-4}$ and $(2.2 \pm 0.3) \times 10^{-4}$ for the ¼- and ½-mil Havar foil cases, respectively. However, we are more interested in the secondary d(t,n) probability per initial

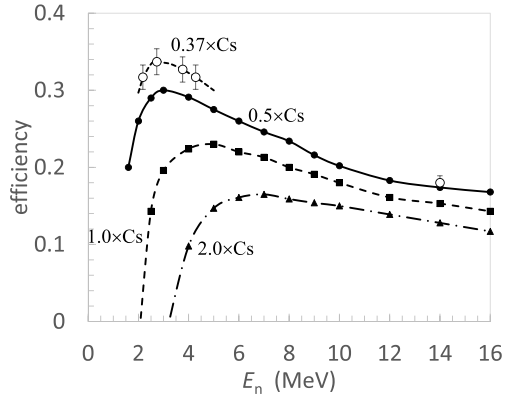

Fig. 9. The detector efficiency. The solid points were read from the efficiency curves from Ref. [9]. The open circles show our extrapolation to a 0.37 × Cs threshold. The error bars show a nominal (conservative) 5% uncertainty. The smooth curves are to guide the eye.

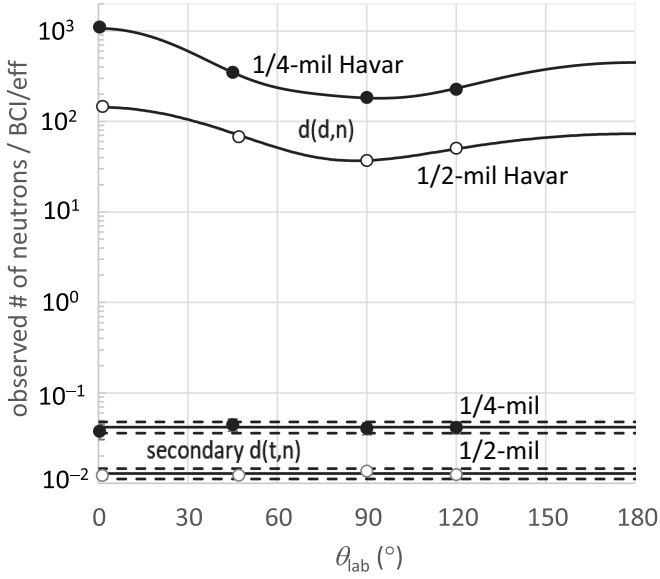

Fig. 10. The angular distribution of d(d,n) neutrons and the secondary d(t,n) neutrons from both the ¼-mil (solid circles) and ½-mil (open circles) Havar foil experiments. The solid curves show the assumed angular distributions. The dashed lines display the uncertainties in the d(t,n) neutrons assuming a flat angular distribution.

d(d,p)t reaction and thus multiply the above ratios by our calculated d(d,n) to d(d,p)t probabilities given earlier. This gives secondary dt-fusion probabilities per initiating d(d,p)t reaction of $(1.7 \pm 0.2) \times 10^{-4}$ and $(2.6 \pm 0.3) \times 10^{-4}$ for the ¼- and ½-mil Havar foil cases, respectively. Please note that these values are for our specific experimental geometry, as the gas cell was not large enough to allow all forward-going and sideways-going d(t,n)-inducing tritons to range out before hitting the edges of the deuterium gas cell (see next section). The quoted experimental errors are predominantly associated with systematic uncertainties associated with our lack of knowledge of the exact nature of the TOF background under and about the dt-fusion neutron peaks and details associated with the true shape of the dt-fusion neutron peaks in TOF space when assessing where to place the assumed background regions on either side of the dt-fusion neutron peaks. Our experimental errors could be reduced by a more detailed model of the expected shape of the TOF spectrum due to dt-fission neutrons and a more detailed assessment of the TOF backgrounds. This type of work was beyond the scope of the present study.

IV. MODEL CALCULATIONS OF SECONDARY IN-FLIGHT D(T,N)α REACTIONS

Here, we calculate the probability of inducing secondary d(t,n)α reactions following initial d(d,p)t reactions

and compare these to the experimental values reported in Sec. III. We have not simply used an existing "off-the-shelf" sophisticated Monte Carlo transport code to set up the geometry of this experiment and automatically compute the secondary reactions, but instead, we compute the probabilities using straightforward hand-calculation methods that can be implemented in a small Excel spreadsheet. This was done, in part, as a follow-on from our recent analysis[4] of Ruhlig's 1938 paper, where we used techniques available only to authors working in the late 1930s to better understand the historical perspective and because our approach better facilitates an understanding of the various processes involved.

To explore the expected properties of the secondary d(t,n)α reactions, we first define a "nominal" initial d(d,p)t reaction to occur at the average interaction depth inside the gas. Later, we will consider perturbations from the nominal case. For the ¼- and ½-mil Havar foil cases, the incident deuterons exiting the Havar foil have average kinetic energies of 1.5 and 0.6 MeV as they enter the gas region, respectively. The average locations for d(d,p)t reactions are 1.5 and 0.3 cm inside the gas cell. For these nominal d(d,p)t reaction locations, Fig. 11 shows the location where the corresponding tritons either hit the edge of the gas cell or range out in the gas. Notice that for the ¼-mil case, the tritons emitted within about 60 deg (90 deg) of the beam direction in the laboratory (center-of-mass) frame run into the edge of the gas cell before ranging out. For the ½-mil Havar case with the lower deuteron energy incident into the gas cell, the above forward angle is reduced to about 30 deg (40 deg). Also, for the ½-mil Havar case, the nominal d(d,p)t reactions are close to the entrance foil, and tritons emitted backward about 160-deg (in the laboratory frame) run into the Havar foil just before they range out in the gas.

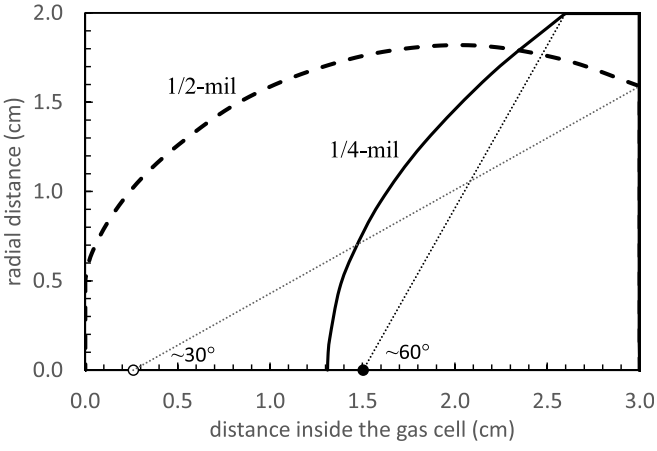

Fig. 11. Some properties of the tritons generated in nominal d(d,p)t reactions. The gas cell is depicted by the solid rectangle, with the Havar foil on the left-hand side of this figure. The vertical axis depicts the radial extent of the gas cell from 0 to 2 cm. The solid (¼-mil Havar foil) and open (½-mil Havar foil) circles show the locations of the nominal d(d,p)t reaction locations. The solid (¼-mil Havar foil) and dashed (½-mil Havar foil) curves show where the tritons emitted from the nominal d(d,p)t reaction sites either hit the edge of the gas cell or range out in the gas.

The initial energies of the emitted tritons for the nominal d(d,p)t reactions depicted in Fig. 11 are displayed in Fig. 12. The probabilities that these tritons induce a d(t,n)α reaction somewhere along their paths inside the gas are shown in Fig. 13. These probabilities are calculated using the method discussed in Sec. II. Notice the discontinuities in the probabilities at 90 and 40 deg in the center-of-mass frames. These angles correspond to the transition (in the forward direction in the laboratory frame) from tritons hitting the edge of the gas cell to ranging out (stopping) in the gas. These probabilities are plotted as a function of the center-of-mass angle of the tritons because it is straightforward to obtain the average probability integrating across the center-of-mass angular distribution of the tritons.[12,13] Converting to laboratory angles before performing the integration is unnecessary because like cross sections, the required average secondary reaction probabilities are invariant observables and do not change between different reference frames.

Integrating the probabilities displayed in Fig. 13 weighted by the relevant triton angular distributions gives the average secondary d(t,n)α reaction probabilities of 1.60×10^{-4} and 2.9×10^{-4} for the nominal d(d,p)t reaction locations for the ¼- and ½-mil Havar cases, respectively. These are still not the final values we seek because we still have to integrate over the distribution of d(d,p)t reaction locations along the symmetry axis of the gas cell. To explore this additional degree of freedom, we have determined the relevant reaction properties at the locations along the incident deuterons' paths where the accumulated d(d,p)t fusion probabilities are 16.7% and 83.3% of the totals. These are representative of the first and last one-third of the d(d,p)t reactions and occur 0.4 and 2.3 cm from the ¼-mil Havar foil, and 0.07 and 0.42 cm from the ½-mil Havar foil. The three d(d,p)t reaction locations representing the midpoints of the first, second, and last one-third fusion regions are displayed in Fig. 14 for the ¼-mil Havar foil experiments. The boundaries of the corresponding triton paths in the gas cell are displayed in the same figure. The corresponding secondary d(t,n)α probabilities integrated along the triton paths inside the gas are given as a function of triton

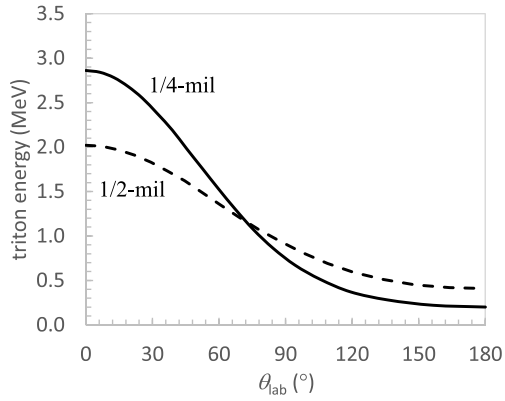

Fig. 12. The initial energy of the emitted tritons in the laboratory frame as a function of the angle to the beam direction in the laboratory frame for the nominal interaction sites displayed in Fig. 11 [¼-mil Havar foil (solid) and ½-mil Havar foil (dashed)].

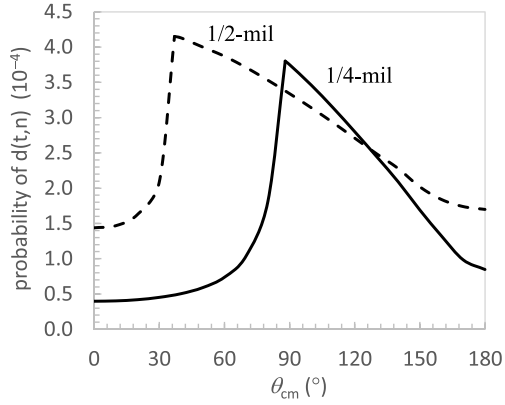

Fig. 13. The probabilities that the tritons summarized in Figs. 11 and 12 induce a d(t,n)α reaction somewhere along their paths inside the deuterium gas as a function of the angle of the emitted d(d,p)t triton in the center-of-mass frame [¼-mil Havar foil (solid) and ½-mil Havar foil (dashed)].

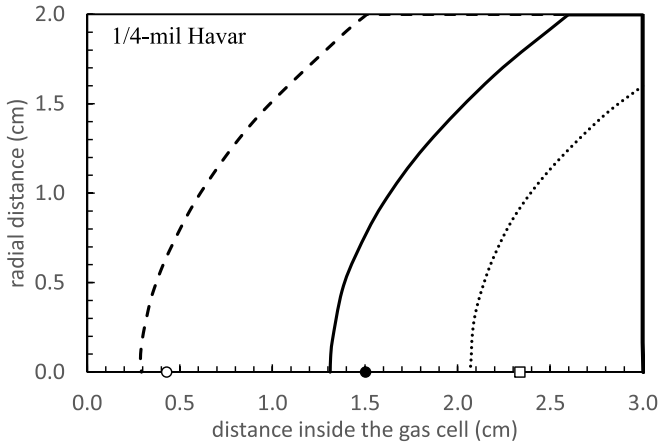

Fig. 14. Some properties of the tritons generated by d(d,p)t reactions in the ¼-mil Havar foil experiments. The gas cell is depicted as in Fig. 11. The dashed, solid, and dotted curves show where the tritons either hit the edge of the gas cell or range out in the gas for the d(d,p)t reaction locations (see text) depicted by the open circle, solid circle, and open square, respectively.

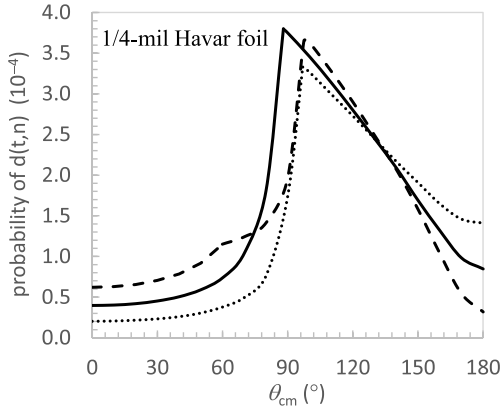

Fig. 15. The probabilities that the triton paths summarized in Fig. 14 (in the ¼-mil Havar foil case) induce a d(t,n)α reaction somewhere along their path inside the gas as a function of the angle of the emitted d(d,p)t tritons in the center-of-mass frame. The inducing tritons are associated with the curve types as displayed in Fig. 14.

emission angle to the beam direction in Fig. 15. The integrals of these weighted by the relevant angular distributions of the tritons are 1.56×10^{-4}, 1.60×10^{-4}, and 1.37×10^{-4} and are displayed in Fig. 16 along with the similarly calculated values for the ½-mil Havar foil case.

A simple average of the three representative d(d,p)t locations gives our estimates for the probability of inducing secondary d(t,n)α reactions of $(1.51 \pm 0.03) \times 10^{-4}$ and $(2.7 \pm 0.1) \times 10^{-4}$ averaged over the initial d(d,p)t reaction sites, for the ¼- and ½-mil Havar foil cases, respectively. These can be compared with the corresponding values of $(1.7 \pm 0.2) \times 10^{-4}$ and $(2.6 \pm 0.3) \times 10^{-4}$ obtained via experiment and reported in the previous section. The quoted theoretical uncertainties of 2% to 4% are associated only with our simple representation of the full distribution of d(d,p)t reaction sites with only three representative locations (see Fig. 16).

The uncertainty in the ENDF-B.VIII[12] evaluated dt-fusion cross sections has been reported to be in the 2% to 3% range.[14] This is partially confirmed by the 2% to 3% differences between the ENDF evaluation and the evaluation of Bosch[11] used here. A significant uncertainty in our calculated RIF secondary dt-fusion probabilities is due to the uncertainties in the used *dE*/*dx* values. If the assumed *dE*/*dx* values are higher/lower than the truth, then the fast ions traverse less/more material, and the

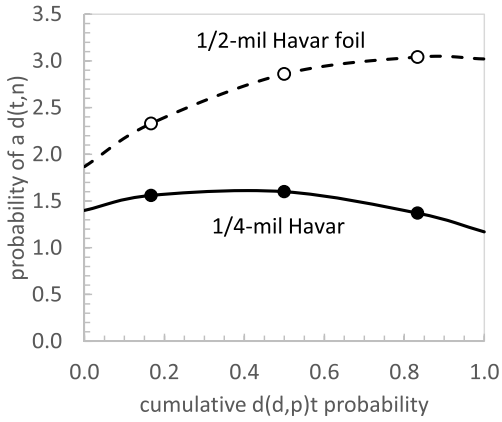

Fig. 16. The calculated probabilities that secondary d(t,n) reactions are generated as a function of the location of the initiating d(d,p)t reaction. This location is here defined by the accumulative fractional probability of the d(d,p)t reaction along the path of the incident deuteron beam. The three calculated points for each Havar foil thickness are representative of the first third, middle third, and last third of the d(d,p)t interaction sites. The curves are to guide the eye and do not represent a detailed calculation.

corresponding fusion probabilities are decreased/increased. We have compared the NIST *dE*/*dx* values used here to the corresponding ones obtained via SRIM.[15] The differences are <0.5% for tritium energies >0.5 MeV but are a few percent in the energy region of interest as the tritons slow down into the dt-resonance region. However, these differences are not reflective of the true uncertainties because of the shared evaluation approaches.

The International Commission on Radiation Units and Measurements[16] has assessed the *dE*/*dx* uncertainties to be 2% to 5% near 1 MeV, but they are in the range of 5% to 10% at lower energies about the dt-fusion resonance. Combining these uncertainties leaves the uncertainties in our predicted dt-fusion probability at about the uncertainties of our experimental probabilities (~10%). A future refinement of the experimental and data analysis technique might make it possible to use measured in-flight dt-fusion probabilities to better test *dE*/*dx* stopping powers in the several hundred kilo-electron-volt region.

V. SUMMARY AND CONCLUSIONS

This work involved the rewarding endeavor of repeating Ruhlig's 1938[2] first-ever reported observation of secondary fusion reactions but was done with modern apparatus under careful laboratory conditions with a deuterium gas target. A comprehensive paper that reports on our follow-on TUNL experiments that use other deuterated compound targets and other detection methods (activation) is under preparation.[5] More information on the importance of Ruhlig's 1938 experiment, and how it launched the United States dt-fusion effort in the 1940s, is provided in another paper in this issue.[14]

We have made the first modern measurement of the probability that tritons emitted in initial d(d,p)t reactions induce secondary d(t,n)α reaction in a well-defined deuterium gas cell at room temperature. The observed secondary probabilities were found to be $(1.7 \pm 0.2) \times 10^{-4}$ and $(2.6 \pm 0.3) \times 10^{-4}$ for 1.5- and 0.6-MeV deuterons, respectively, incident on 4.05 atm of deuterium in a cylindrical gas cell with a length of 3 cm and a diameter of 4 cm. The finite extent of the gas cell causes the higher-energy deuteron case to give a lower secondary d(t,n) probability. This is because in the higher-energy case, the initiating d(d,p)t reactions occur across the whole length of the gas cell and because with the higher center-of-mass velocities, a significant fraction of the forward-going tritons hits the front edge of the gas cell before their kinetic energies are degraded into the dt-fusion resonance region (see Fig. 5).

The relevant secondary dt-fusion probabilities are calculated using ion stopping powers,[10] fusion cross sections,[11] and d(d,p)t angular distributions[12,13] available in the literature. The corresponding theoretical probabilities for our specific experimental geometry are $(1.51 \pm 0.03) \times 10^{-4}$ and $(2.7 \pm 0.1) \times 10^{-4}$ for the 1.5- and 0.6-MeV deuteron cases, respectively, and are in agreement with our experimental observations. These results add confidence to the assumed stopping powers and the used numerical methods. This adds verification and validation to parts of the recent analysis of Ruhlig's 1938 experiment on secondary reactions, published in this same issue.[4]

Acknowledgments

We thank Mark Paris for information on light fusion reaction angular distributions and Sean Finnegan and Nate Sanchez for their support.

Disclosure Statement

No potential conflict of interest was reported by the author(s).

Funding

This work was supported, in part, by the National Nuclear Security Administration Stewardship Science Academic

Alliances, grant number [DE-NA0004076], and the U.S. Department of Energy, Office of Nuclear Physics, under grant number [DE-FG02-97ER41033].

ORCID

M. B. Chadwick http://orcid.org/0000-0003-3017-6050

References

1. A. HAYES et al., "Reaction-in-Flight Neutrons as a Test of Stopping Powers in Degenerate Plasmas," *Phys. Plasmas*, **22**, *8*, 082703 (2015); https://doi.org/10.1063/1.4928104.
2. A. J. RUHLIG, "Seach for Gamma-Rays from Deuteron Deuteron Reaction, Letters to the Editor," *Phys. Rev.*, **54**, *4*, 308 (1938); https://doi.org/10.1103/PhysRev.54.308.
3. D. B. SAYRE et al., "Neutron Time-of-Flight Measurements of Charged-Particle Energy Loss in Inertial Confinement Fusion Plasmas," *Phys. Rev. Lett.*, **123**, *16*, 165001 (2019); https://doi.org/10.1103/PhysRevLett.123.165001.
4. J. P. LESTONE et al., "Ruhlig's 1938 First-Ever Observation of the Fusion of $A = 3$ Ions with Deuterium: An Analysis of Secondary Reactions Following Deuteron-on-Deuterium Fusion in a Heavy Phosphoric Target," *Fusion Sci. Technol*. (2024).
5. J. B. WILHELMY et al., "Triton-Deuteron Reaction-in-Flight Studies via Deuteron Interactions with D_2O, CD_2, and D_3PO_4" (2024) (to be submitted for publication).
6. TUNL FN Tandem Accelerator website; https://tunl.duke.edu/research/our-facilities.
7. H. BETHE, "On the Theory of the Passage of Rapid Charged Particle Radiation Through Matter," *Ann. Der. Physik*, **5**, 325 (1930).
8. D. W. GLASGOW et al., "A High-Precision Neutron Time-of-Flight Facility," *Nucl. Instrum. Methods*, **114**, *3*, 541 (1974); https://doi.org/10.1016/0029-554X(74)90180-3.
9. R. S. PEDRONI, "Cross Sections and Analyzing Powers in the 8- to 17-MeV Range for Neutron Scattering from ^{54,56}Fe, ^{58,60}Ni and ^{120}Sn," PhD Thesis, p. 60, Duke University (1986); https://nucldata.tunl.duke.edu/nucldata/Theses/TUNL_Theses.shtml#1986.
10. M. J. BERGER et al., "ESTAR, PSTAR, and ASTAR: Computer Programs for Calculating Stopping-Power and Range Tables for Electrons, Protons, and Helium Ions," Version 1.2.3, National Institute of Standards and Technology (2005); http://physics.nist.gov/Star (current as of Sep. 15, 2022).
11. H. BOSCH, "Review of Data and Formulas for Fusion Cross-Sections," IPP I/252, Max-Planck-Institute for Plasma Physik (Sep. 1990).
12. D. A. BROWN et al., "ENDF/B-VIII.0: The 8th Major Release of the Nuclear Reaction Data Library," *Nucl Data Sheets*, **148**, *1* (2018).
13. H. LISKIEN and A. PAULSEN, "Neutron Production Cross Sections and Energies for the Reactions T(p,n)^{3}He, D(d,n)^{3}He, and T(d,n)^{4}He," *Nucl. Data Tables*, **11**, *7*, 569 (1973); https://doi.org/10.1016/S0092-640X(73)80081-6.
14. M. B. CHADWICK et al., "Early Nuclear Fusion Cross-Section Advances 1934–1952 and Comparison to Today's ENDF Data," *Fusion Sci. Technol*. (2024).
15. J. F. ZIEGLER, SRIM-2013 software website, www.srim.org.
16. "Stopping Powers and Ranges for Protons and Alpha Particles," ICRU Report 49, International Commission on Radiation Units and Measurements (1993).